https://doi.org/10.1016/j.compscitech.2021.109195

Three-dimensional Composites with Nearly Isotropic Negative Poisson's Ratio by Random Inclusions: Experiments and Finite Element Simulation

Minglonghai Zhang [a], Hong Hu [a]*, Hasan Kamrul [a], Shuaiquan Zhao [a], Yuping Chang [a], Mabel Ho [b], Nazmul Karim [c]

[a] Institute of Textiles and Clothing, The Hong Kong Polytechnic University, Hong Kong, China

[b] Industrial Centre, The Hong Kong Polytechnic University, Hong Kong, China

[c] Centre for Fine Print Research, The University of West of England, Bristol, UK

Abstract

Composites with negative Poisson's Ratio (NPR), also known as auxetic composites, are of great interests due to excellent properties. Auxetic composites of various types have been developed, however most of them have anisotropic NPR behaviour. This paper reports a new type of three-dimensional (3D) composites with nearly isotropic NPR by randomly embedding rigid re-entrant equilateral triangle inclusions into soft matrix. Four types of inclusions with different structural parameters including re-entrant angle, prism length and rib thickness were first made from two types of carbon fibre prepregs, and then embedded into silicone rubber matrix with different inclusion numbers to fabricate 3D composites with various volume fractions of inclusions. Both experimental and finite element analyses were conducted to investigate the deformation behaviours under compression and the effects of different structural parameters and materials. The results show that the NPR of the composites can be realised with suitable structural parameters and properties. The lowest NPR of -0.19 was obtained via embedding 6mm length inclusions made of one-layer 3K twill weave carbon fibre prepreg with an inclusion number of 800. The study provides a new approach for the development of 3D composites with isotropic NPR for the practical applications of auxetic materials.

Corresponding author:

Hong Hu; Email: hu.hong@polyu.edu.hk

Keywords: Auxetic composite, C. Deformation C. Finite element analysis, B. Mechanical properties

1. Introduction

The materials with negative Poisson's ratio (NPR) are known as auxetic materials. They have attracted great scientific interests since the first manmade auxetic material was reported in 1987 [1]. In contrast to conventional materials, auxetic materials contract transversally when they are axially compressed or expand transversally when they are axially stretched [2]. Such unusual deformation behaviour results in unique mechanical properties of the auxetic materials. It has been found that the auxetic materials have better indentation resistance [3, 4], enhanced energy absorption [3-6], increased shear modulus [7], synclastic curvature [8] and shape fitting ability [9], when compared with conventional materials. Due to their incredible properties, auxetic materials are very promising for many applications. The examples include smart drug delivery bandages, medical stents, sensors, protective equipment, energy absorption materials, filters with adjustable permeability, fasteners, acoustic dampers and so on [10, 11].

Among various manmade auxetic materials, many researches have been focused on auxetic composites and structures due to their good specific strength and modulus, and other properties [12-14]. In addition, properties and structures of composites can be designed to manufacture strong and light-weight materials by using high performance fibres. Two different approaches have been developed to manufacture auxetic composites so far [9]. The first one is to use conventional manufacturing technique and non-auxetic materials to produce auxetic angle-ply laminates with special laminating orientation. However, the auxetic behaviour of the auxetic angle-ply laminates can only be achieved in certain directions of the composite due to the intrinsic structural limitations of laminates [13-16]. The second approach is to make auxetic composites by using special designed auxetic reinforcements such as auxetic yarns [17, 18], auxetic fabrics [19, 20] and inclusions [21-23] or fabricating the composite with auxetic geometry including modified orthogonal structure [24], re-entrant structure [25, 26], chiral

structure [6, 27] and double-arrow-head structure [28-30] etc. Both two-dimensional (2D) and three-dimensional (3D) auxetic composites have been designed through the second approach. However, the auxeticity of such composites are limited to certain directions leading to anisotropic behaviour which limits potential applications of auxetic composites. Moreover, the mechanical properties of most 3D auxetic composites reported are relatively weak, as the polyurethane is used as the matrix [24]. The 3D auxetic composites embedded with inclusions in different shapes and structures such as re-entrant structures, rigid rotating squares, ellipses, ellipsoids, spheres and cubes have been theoretically studied and analysed by various researchers using both analytical and numerical methods [21, 23, 31, 32]. It is believed that the NPR could be realised when the auxetic inclusion volume fraction exceeds a critical value and the difference of the Young's modulus between the inclusions and the matrix is high enough to a certain value [33, 34]. The auxetic composite embedded with auxetic inclusions are believed to be able to realise isotropic NPR, and they can be applied in many areas such as automobile, civil engineering, sport equipment and many others. However, this type of auxetic composites have only been theoretically studied and numerically simulated yet[21, 23, 31-35]. The real composites with isotropic NPR using inclusions are not found in the current literature.

In this study, 3D composites with nearly isotropic NPR were produced by using re-entrant triangle prisms made of carbon fibre prepregs as inclusions, and silicone rubber as matrix. The inclusions were randomly distributed in the silicon matrix with an intention of creating nearly isotropic NPR behaviour. A series of composite samples were fabricated with different parameters including inclusion number, re-entrant angle, rib thickness, prism length and type of fibre prepregs in order to understand their effects on deformation behaviour of composites. All samples were subjected to quasi-static compression tests to measure their compression behaviour and auxeticity. The finite element (FE) analysis was also conducted to simulate the deformation behaviour and auxetic performance of the composites and compare with the experimental results.

2. Experimental

2.1. Structure of inclusions

The structure of inclusions is the most important factor to be discussed before fabricating 3D auxetic composites. To date, it is possible to manufacture different auxetic geometries via different processing methods such as 3D printing technology [26]. However, 3D printing is not suitable to produce 3D composites with hollow inclusions due to enclosed void spaces. According to the previous studies [33-35], both re-entrant equilateral triangle and regular tetrahedron are able to provide 2D and 3D composites with isotropic NPR, but the regular tetrahedron is difficult for manufacturing. Therefore, the re-entrant equilateral triangle prism was chosen in this research. Fig. 1(a) shows the schematic diagram of a re-entrant equilateral triangle inclusion used. As shown in Fig.1(b), when the re-entrant equilateral triangle unit is compressed along all its symmetry axes, the ribs move toward the centre of the re-entrant triangle leading to a lateral contraction of the overall composite, thus the auxetic effect is achieved. On the other hand, when the re-entrant equilateral triangle unit is compressed in any other directions between any symmetry axes, it exhibits similar deformation behaviour because of the component forces along the symmetry axes and the intrinsic property of the equilateral triangle. As a result, the 3D composite embedded with re-entrant equilateral triangle inclusions is possible to have nearly isotropic Poisson's ratio (PR). The re-entrant angle α, prism length l, rib length w and rib thickness δ of the inclusion are believed to be the key geometrical parameters affecting the auxetic performance as they can directly influence the inward movement of inclusion ribs when the composite is compressed. In order to obtain isotropic PR and mechanical properties of the 3D composite embedded with inclusions, the inclusions are designed to be randomly distributed and oriented in the composite matrix.

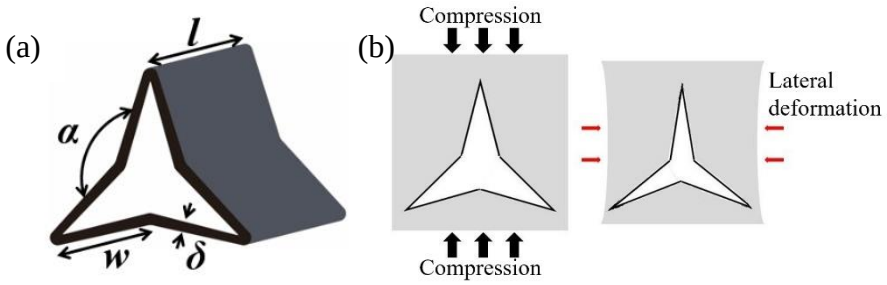

Fig. 1 (a) Re-entrant equilateral triangle inclusion, (b)deformation of the re-entrant triangle.

2.2. Materials and fabrication procedure

According to the previous study [33], the difference of Young's moduli between the inclusions and matrix should be high enough to create the NPR of the composite. In addition, the inclusions need to have flexibility to allow inward movement of ribs when the composite is compressed. To satisfy the requirements of both modulus difference and flexibility, T300 3K twill weave carbon fibre prepregs with 200 gsm and T300 1k plain weave carbon fibre prepregs with 90 gsm purchased from Chicken's Carbon Fibre Ltd. were used to make the inclusions respectively. Both twill weave and plain weave carbon fibre prepregs cab provide high mechanical properties along orthogonal directions of the prepreg, but relatively weak mechanical performance along the thickness and bias directions of the prepreg, which brings flexibility of the inclusions. To guarantee the flexibility of the ribs, only one layer of 3K carbon fibre prepreg were used for making inclusion, and three layers of 1K carbon fibre prepreg were used to make inclusion with similar rib thickness and higher modulus. KE-1310ST high strength silicone rubber purchased from Shin-Etsu Chemical Co. Ltd. was selected as the matrix because the combination of the carbon fibre/epoxy laminate and the silicone rubber could create a relatively large stiffness difference and the silicon is soft enough to deform under compression. Furthermore, the viscosity of the silicone rubber is very high, which can prevent floating up or sink down movements of inclusions before the silicone rubber is cured. The properties of the carbon fibre laminates and silicone rubber were measured following ASTM D3039-17 and ASTM D575-1991(2018) respectively. The measured properties are listed in

Table 1, except that the v value of the silicone was provided by the supplier for the reference.

Table 1 The properties of materials

Property	1-layer 3K carbon fibre laminate	3-layers 1K carbon fibre laminate	Silicone rubber
E_1 (GPa)	7.3	9.7	0.0027
E_2 (GPa)	7.3	9.7	\
E_3 (GPa)	1.1	1.72	\
G (GPa)	0.63	1.16	\
v	0.21	0.19	0.5
Density (g/cm^3)	1.2	1.21	1.08

The fabrication process of the composite with inclusions is schematically illustrated in Fig. 2(a). First, long re-entrant equilateral triangle prism is manufactured by using carbon fibre prepreg. Then the long prism is cut to make short inclusions and the two ends of the inclusions are sealed by using soft sealant. Finally, the inclusions are mixed with silicone rubber to make the final 3D composite. In this manufacturing process, it is extremely difficult to directly make re-entrant equilateral triangle prism using carbon fibre prepreg and 3D re-entrant equilateral triangle mould, because the modulus of the carbon fibre is so high that the carbon fibre prepreg cannot be curved to fit the mould with re-entrant equilateral triangle shape. In addition, as the carbon fibre prepreg will be forced to tightly contact with the mould by the vacuum pump in a 3D shape, the cured composite cannot be easily demoulded from the mould. Thus, in this research, a three-stages process was adopted. First, the laminate is manufactured on a stainless-steel mould with wave surface (Fig. 2(b) and (c)) under a high pressure, which makes laminate plate with wave shape. Then, the plate is cut to make V-shape strips. Finally, every three strips are adhered together on a 3D stainless-steel re-entrant equilateral triangle mould to form the final inclusion.

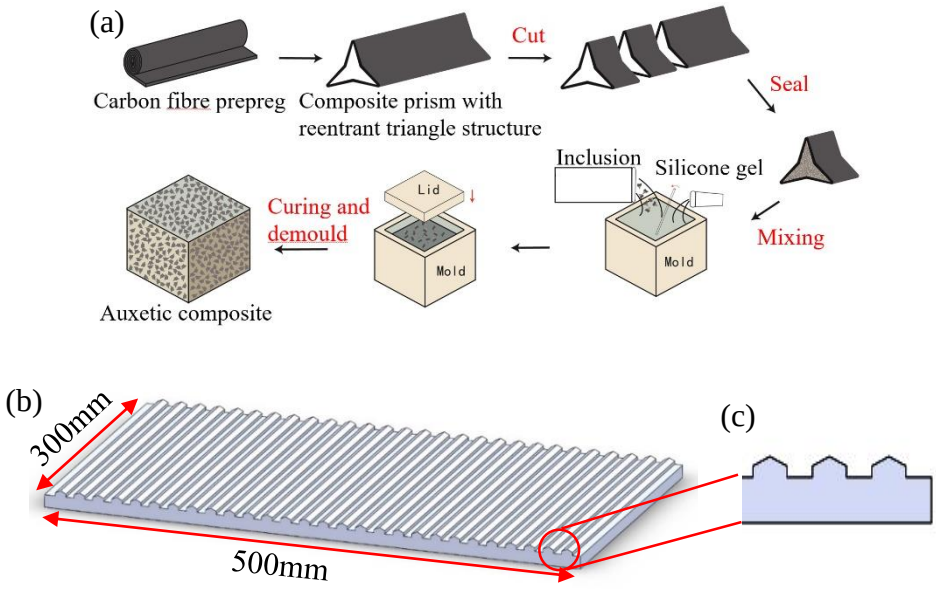

Fig. 2 (a) Schematic diagram showing the manufacturing process of 3D auxetic composite, (b) schematic diagram of the wave-surface mould, (c) cross-section of the mould.

2.3. Inclusion manufacturing

As shown in Table 2, four types of inclusions with different structural parameters and carbon fibre prepregs were made using the three-stages process. The rib lengths of all inclusions were selected as 4.07 mm which was the shortest length could be manufactured. In the first step, the wave shape carbon fibre laminate was manufactured according to the conventional prepreg composite laminating process. The prepregs were cured under the maximum of 130 °C curing temperature with a temperature increasing and decreasing rate of 1.5 and a pressure of 150 psi for 2 hours. Once the curing had finished, the assembly was taken out of the autoclave and the cured carbon fibre laminate was demoulded from the wave surface mould. In the second stage, the wave laminates were cut by using ProtoMAX water jet cutting machine (Omax Ltd.) to make V-shape strips. Then, the cut V-shape strips were washed in deionised water to clean the abrasive sands and dried in an oven for 24 hours at 60 °C. In the final stage, the methyl methacrylate structural adhesive (VuduGlu VM100 from Easy Composites Ltd.) was applied onto the edges of each strips and every three strips were stuck together on a 3D re-entrant equilateral triangular mould to obtain the re-entrant equilateral triangular prism with the right

size and angle. The prisms were then cut by ProtoMax water jet cutting machine to get shorter prisms with 6 mm or 8 mm length. The cut prisms were also cleaned in the deionised water and dried in the oven for 24 hours at 60 °C. Finally, the two ends of these prisms were sealed by the PU18 high strength soft polyurethane sealant from BOND IT Ltd.

Table 2 Types of inclusions produced

Inclusion	Fibre prepreg	Laminating layers	Re-entrant angle α (°)	Rib length W (mm)	Prism length l (mm)	Rib thickness δ (mm)
Type 1	1K plain weave	3	149	4.07	6	0.5
Type 2	3K twill weave	1	149	4.07	6	0.4
Type 3	3K twill weave	1	149	4.07	8	0.4
Type 4	3K twill weave	1	159	4.07	6	0.4

2.4. Composite manufacturing

The silicone rubber gel, catalyst and inclusions were first added into a plastic bucket, and then mixed by an electric stirrer for 10 mins to get a homogeneous mixing which allowed the inclusions to be randomly distributed in the rubber gel. Following to the mixing, the silicone rubber gel was placed into a high-power vacuum chamber for 5 mins to degas the silicone rubber. After the degassing, the silicone rubber gel with inclusions was added into the mould and the assembly was put into the vacuum chamber for the second degassing. Then the mould was taken out of the vacuum chamber and covered by an acrylic plate to flatten the upper surface of the silicone gel. The whole assembly was placed in laboratory ambient temperature of 25 °C for 24 hours to cure. After that, the cured composite was demoulded. Four groups of auxetic composites were manufactured by using Type 1, Type 2, Type 3 and Type 4 inclusions, respectively. Each group of auxetic composites was manufactured with 400, 500 and 600 inclusions respectively. Two extra composite samples with Type 2 inclusions were

manufactured with 700 and 800 inclusions to study the maximal inclusions that can be added. The composites with different types and numbers of inclusions are named as C1-400 to C1-600, C2-400 to C2-800, C3-400 to C3-600 and C4-400 to C4 600 respectively. The volume fractions of the inclusion shell, silicone and voids are shown in Table 3. One pure silicon sample was also prepared for comparison.

Table 3 The volume fraction of inclusion shell, silicon and voids (%)

Composite	C1-400	C1-500	C1-600	C2-400	C2-500	C2-600	C2-700	C2-800	C3-400	C3-500	C3-600	C4-400	C4-500	C4-600
Inclusion shell	5.9	7.3	8.8	4.7	5.9	7.0	8.2	9.4	6.3	7.8	9.4	4.7	5.8	7.0
Silicon	86.1	82.6	79.1	87.2	84.0	80.6	77.7	74.5	83.0	78.7	74.5	87.2	84.0	80.8
Void	8.1	10.1	12.1	8.1	10.1	12.1	14.1	16.2	10.8	13.5	16.2	8.2	10.2	12.2

2.5. Quasi-static compression test

To assess the auxetic behaviour and compressive performance, all the 3D auxetic composite samples and pure silicone rubber sample were subjected to compression tests on an Instron 5566 universal testing machine with two 150 mm compression circular plates. The compression tests were conducted following the standard test methods for rubber properties in compression (ASTM D575-1991(2018)) since the silicone rubber was the matrix material of composite samples. The dimensions of each composite were 100 mm x 100 mm x 50 mm. Prior to the compression test, one square side and one rectangle side of each sample were marked with a cross in the centre of the sample and all the samples were kept in the laboratory ambient environment (temperature of 23 °C, relative humidity of 65 %) for 3 hours. The measurement setup is shown in Fig.3. Two sheets of sandpaper (8 × 13 cm) were used between the silicone rubber surfaces and the compression circular plates surfaces to prevent the lateral slippage of the silicone rubber at the contact surfaces. The compression stresses and strains were directly obtained from the Instron machine. To measure the lateral and vertical displacements of the

composite sample, a Canon camera was placed 50 cm in front of the sample to record the whole compression procedure for each test. The marked face was placed toward the camera. Each sample was compressed along the *y* direction of the sample for three times till 20% of the compression strain and the results of the third compression was collected. Then, the median results of three samples were obtained to calculate the value following the procedure required by the ASTM D575-1991(2018) standard. The compression speed was set as 12 mm/min. To measure the isotropic property of the composite samples, the same measuring procedure was also applied to all composite samples along the x and z directions, respectively. As pure silicone rubber is isotropic, it was only compressed in one direction to measure PR. After the compression test, the videos recorded were processed by using KMPlayer to extract photos with 1 second interval. Then a screen ruler of FastStone Capture was used to measure the height (*H*) and width (*W*) of the composite through measuring the cross from the beginning to the end of the tests. To minimise the boundary effect, only the displacement in the centre area along the cross marked is measured as shown in Fig.3(b).

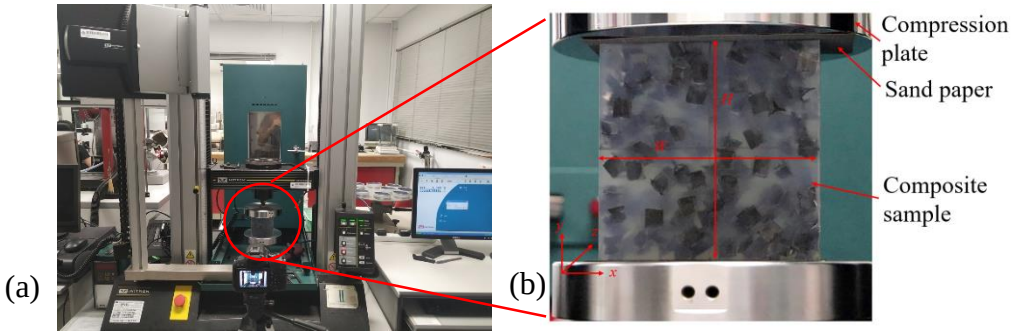

Fig. 3 (a) Experimental setup of the compression test, (b) composite under compression.

From the measured *H* and *W*, the compression strain (ε_c) was calculated from $\varepsilon_c=(H-H_0)/H_0$ and the lateral strain (ε_l) was calculated from $\varepsilon_l=(W-W_0)/W_0$, where H_0 and W_0 are the original height and width of composites. The PR (v) of the composite was then obtained from $v=-\varepsilon_l/\varepsilon_c$.

3. Finite element modelling

The 3D auxetic composites were modelled by using the SOLIDWORKS 3D CAD 2017 software, and the coordinates and orientation of inclusions were randomly generated by Python

3.8. A generated model is shown in Fig. 4(a). Once the models were generated, they were imported to ABAQUS/Standard 2017 for FE analysis. The standard static analysis was conducted. The linear elastic material model was used for both inclusion and matrix, and the types for inclusion and matrix were ‘engineering constants’ and ‘isotropic’, respectively. The engineering constants of the materials are designated according to Table 1. The interface between each V-shape plates was set to be tied. Therefore, every three connected V-shape plates could act as one inclusion. The interface between each inclusion and the matrix was set to be tied as well to facilitate convergence. For the boundary conditions, all nodes located in the bottom were fixed in all directions, and all nodes in the top surface were fixed in x and z direction to simulate the real compression process. The compression force was set to apply on the nodes in the top surface along the y direction with a fixed distance of 20 mm. To generate meshes with good quality, tetrahedron elements were chosen for all models. The mesh size was set to be 1 mm and 2 mm for inclusions and matrix respectively after the mesh convergence study. Fig. 4(b) shows the whole meshed model and Fig. 4(c) shows the meshed model of inclusions. The displacements of nodes A and B in y direction and the displacements of nodes C and D in x direction were exported for calculating compression strain ε_c and lateral strain ε_l, respectively. The same modelling procedure was conducted for all types of 3D auxetic composite samples. In addition, composites with 200 and 300 inclusions of Type II were also modelled and analysed to get a better understanding of the inclusion number on the effect of the deformation behaviour of the composites.

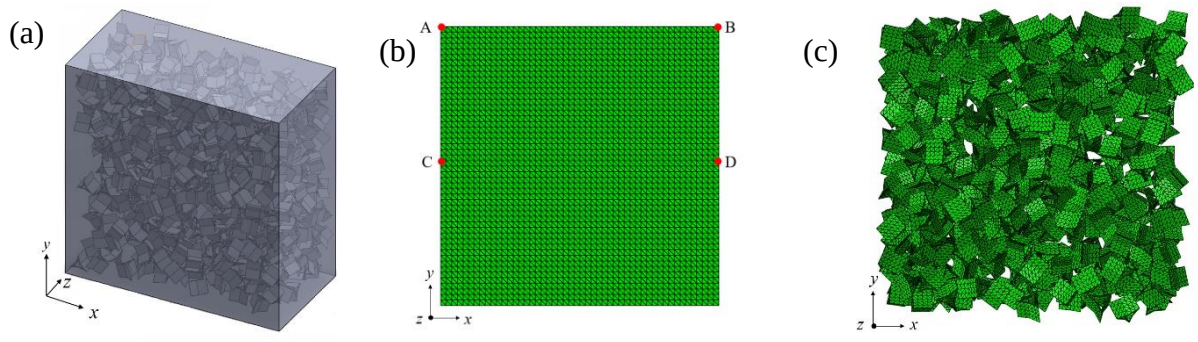

Fig. 4 (a) Model of the auxetic composite embedded with inclusions, (b) FE model for

compression tests, (c) FE model without matrix.

4. Result and discussion

4.1. Deformation behaviour of 3D auxetic composites

To facilitate the analysis, 3D composite C2-500 is first selected as an example to discuss the typical deformation behaviour of the 3D auxetic composites under compression. Its PRs in three directions (x, y and z) as a function of the compression strain from the experiment are shown in Fig. 5, in which the PR curve of the pure silicon is also plotted for comparison. It can be seen that the pure silicon only exhibits positive PR and its PR is not constant and increases with the compression strain, which is different from the value provided by the manufacturer as listed in Table 1. The PR curves of the composite show that the embedding of re-entrant equilateral triangle inclusions can lead to the reduction of its PR from positive to negative, and the NPR behaviour is realised during the initial stage of compression from 2% to around 6% compression strain. As expected, the composite has nearly isotropic PR because the curves in three directions are almost coincided. However, some small differences are still noted among the three curves. This phenomenon can be explained by the anisotropic properties of the inclusions, inconsistent deformations of inclusions in the three directions and their incompletely random distribution and orientation in the matrix. For example, when the composite is compressed along y direction, the axial directions of inclusions may be aligned with the y direction, x direction or z direction or may be tilted to these directions. The inclusions having the axial direction aligning with y direction cannot contribute to the lateral deformation of the composite under y compression as they cannot be compressed in the radial direction. The inclusions aligned with x direction can only provide z direction deformation of the composite. On the contrary, the inclusions aligned with z direction will provide x direction deformation of the composite. The tilted inclusions deform according to their positions and orientations and may gradually provide x direction deformation of the composite as the

component force applied toward the radial direction of the tilted inclusion is much smaller than the compression force. Therefore, to enhance the isotropy of NPR of the composite, inclusions with a structure having more consistent deformation behaviour in all directions and their completely random distribution in the matrix are highly required.

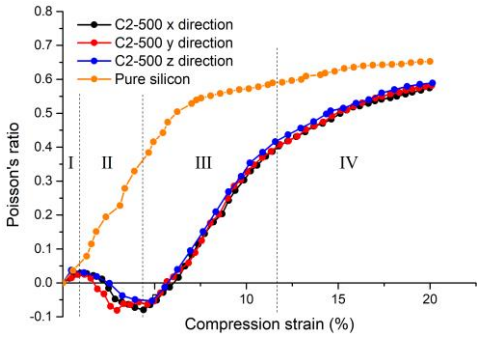

Fig. 5 PR-compression strain curves of C2-500 composite along x, y and z directions.

From Fig. 5, it can be also seen that the PR of the composite is not constant and its variations as a function of compression strain can be divided into four stages. The stage I starts from very beginning of compression process to a compression strain of about 1%. In this stage, the PR of the composite slightly increases with compression strain and reaches its first peak point with a value of about 0.25. During this stage, the inclusions do not deform or only deform to a very small extent, and the composite slightly expands in the lateral direction due to larger expansion of silicone than total shrinkage produced by inclusions. The stage II starts from the first PR peak point to the second peak point. In this stage, the PR starts to decrease from positive to negative and reaches its maximal NPR at a compression strain of about 4.0%. During this stage of compression, more inclusions start to deform inward and their inward deformation continues to increase with the compression strain. When the total inward deformation of inclusions exceeds the lateral expansion of silicone, the PR of the composite becomes negative. The NPR continues to increases until its maximal value when the inclusions achieve their maximal inward deformation. Fig.6 shows the lateral deformations of the composite at different compression strains from both the experiment and FE simulation. From the magnified image of Fig. 6(a) and (b), it can be confirmed that the composite laterally contracts at a compression

strain of 4%. The deformed width l_1 is smaller than the original width l_0. The stage III starts from the maximal NPR to the turning point at a compression strain of about 12%. In this stage, the PR starts to increase, changing from negative to positive. The PR becomes 0 when the compression strain reaches about 6.5%. With further compression, the lateral expansion of silicone gets much important than the total inward deformation of inclusions and the PR rapidly increases to a value of 0.4 when the compression strain reaches 12%. The stage IV starts from the turning point to the end of compression process. In this stage, the PR of the composite continues to increase but with a smaller increase rate due to reduction in the increasing rate of PR of silicone. At the end of the compression process, the PR value reaches 0.58, which is very close to that of the silicone, which is 0.65. Fig. 6(c) and (d) confirm the lateral expansion of the composite after the PR becomes positive.

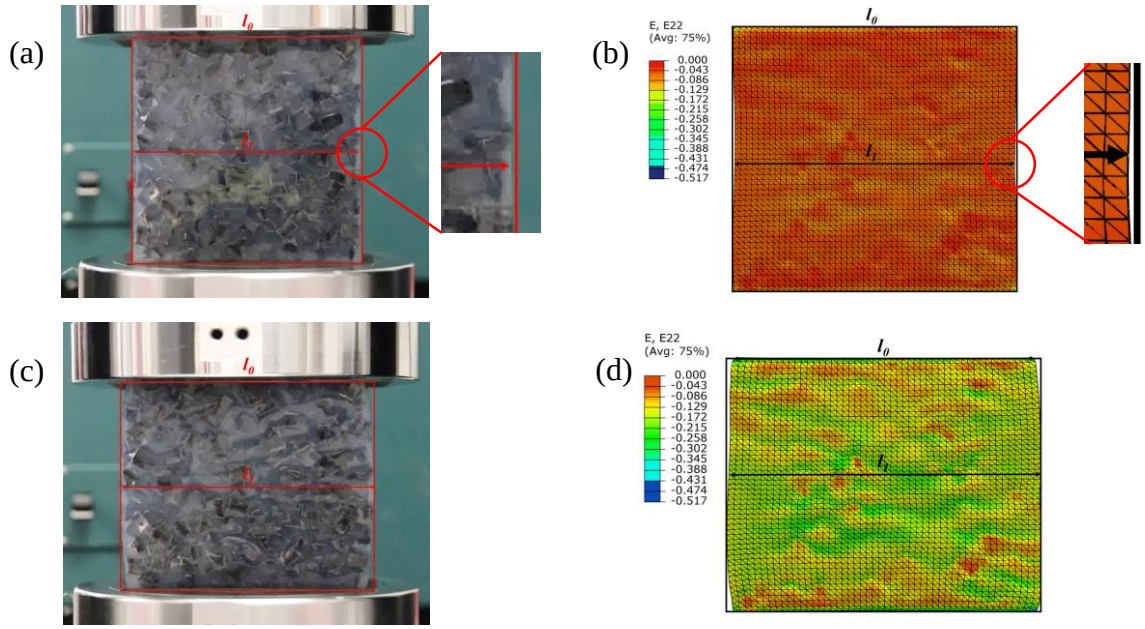

Fig. 6 Deformations of C2-500: (a) and (b) test and FE simulation at 4% compression strain, (c) and (d) test and FE simulation at 15% compression strain.

4.2. Effect of inclusion number

The FE simulated and experimental PR-compression strain curves of the C2 composites made with the same type of inclusions but with different inclusion numbers (200 to 800 for FE simulation and 400 to 800 for experiment) are shown in Fig. 7(a) and (b). In order to get a

better comparison, the largest NPR values obtained from both the experiment and FE simulation are also plotted against inclusion number, as shown in Fig. 7(c). It can be seen from Fig. 7(a) that, when the inclusion number is 200 or 300, the composite does not exhibit NPR or only has very small NPR. Therefore, to facilitate the composite fabrication, only composites with 400 inclusions or above were fabricated. It can be also observed that the NPR behaviour of the composites increases with increasing inclusion numbers. However, after the inclusion number is more than 700, the inclusions become overcrowded in the matrix leading to extra expansion of the composite and higher increase rate of PR after the compression exceeds 17% of compression strain. From Fig. 7(a) and (b), it is also noted that the range of compression strain having NPR gets larger with higher inclusion numbers. The composites can even achieve NPR since the beginning of the compression process after their inclusion numbers exceed 700 like C2-700 and C2-800. The influence of the number of inclusions is resulted from the intrinsic deformation mechanism of the composites. The composite can laterally contract when the total inward deformation of the inclusions exceeds the lateral expansion of silicone. The composite embedded with more inclusions can have more total void space inside the inclusions, which is able to provide larger space for the lateral contraction of the composites. As shown in Table 3, the volume fraction of void space increases from 8.1% to 16.2% when the inclusion numbers increase from 400 to 800 for C2-400 to C2-800. The maximal NPR is also increased from -0.07 to -0.20. Thus, the composite with more inclusions can have better auxeticity. On the other hand, decreasing inclusion number can lead to positive PR. To get the NPR, the inclusion number should exceed a minimum number when other parameters are kept unchanged.

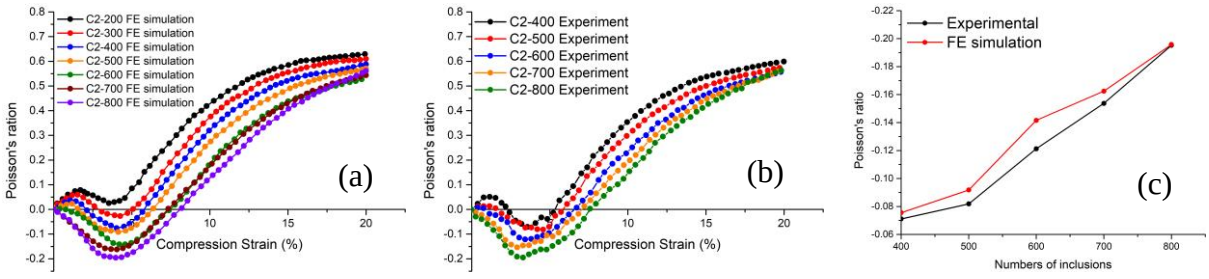

Fig. 7 (a) and (b) FE simulated and experimentally measured PR-compression strain curves

with different inclusion numbers, (c) variation of the largest NPR with inclusion numbers.

As presented in Fig. 7(a) and (b), the FE simulated results match well with the experimental results and the PR curves obtained from both cases have a similar variation trend with the increase of inclusion numbers. However, it is noted from Fig. 7(c) that the largest NPRs from the FE simulation are a little lower than those from the experiment. This reason can be explained by the ignorance of sealing part at two ends of inclusions in the FE modelling. As the manufactured inclusions have to be sealed with soft sealant to prevent intrusion of silicone rubber during the curing period, the sealant makes inclusions stiffer and limit the inward deformation of the re-entrant triangle. However, in FE simulation, the two ends of each inclusion are not covered sealant to simplify the modelling and to facilitate convergence. In addition, the interfaces between inclusions and silicon matrix of FE models are set to be tied, which means there is no free degree between these two contact faces and they cannot be separated. But in the composites manufactured, these two contact faces cannot be perfectly bonded together due to the existence of weak points. Moreover, the variations of PRs of FE models are more even compared with the experimental results.

4.3. Effect of fibre prepregs and laminating layer

Both the experimental and FE simulated PR-strain curves of the composites (C1-400 to C1-600 and C2-400 to C2-600) made with the inclusions of the same re-entrant angle, the same rib length and the same prism length but with different carbon fibre prepregs and laminating layers (3-layers 1K plain weave carbon fibre prepreg and 1-layer 3K twill weave carbon fibre prepreg) are shown in Fig. 8, in which the PR curve of the pure silicon is also plotted for comparison. It can be seen that all C1 composites made from 3-layers 1K plain weave carbon fibre prepreg do not exhibit any auxetic effect although their PR is reduced compared with that of the silicone matrix due to embedding of inclusions, especially in the second stage of compression. There are three reasons for explaining this non-auxetic behaviour of the C1 composites. First, as

shown in Table 1, the laminates made from 3-layers 1K plain weave carbon fibre prepreg have higher moduli in three principal directions compared with those made from 1-layer 3K twill weave carbon fibre prepreg, which makes the inclusions stiffer in these directions. Second, the rib thickness of inclusions for C1 composites is thicker than that of C2 composites, which can result in higher bending modulus of the laminate and less flexibility of the ribs of inclusions. The bending modulus (K) of the inclusion at the re-entrant point can be calculated:

$$K = E_2 \frac{l\delta^3}{12} \tag{1}$$

where E_2 is the Young's modulus of the laminate, l and δ are the prism length and rib thickness of the inclusion. It is clear that the increase of E_2 and δ will lead to the increase of bending modulus. Third, the plain weave structure has less flexibility than the twill weave structure, which also contributes to the structure stability of laminate. Therefore, the inclusions made of the 1K plain weave carbon fibre prepreg become more difficult to deform inward under compression to provide NPR effect of the composites. The results show that selecting suitable material and rib thickness is very important to achieve the NPR of composites.

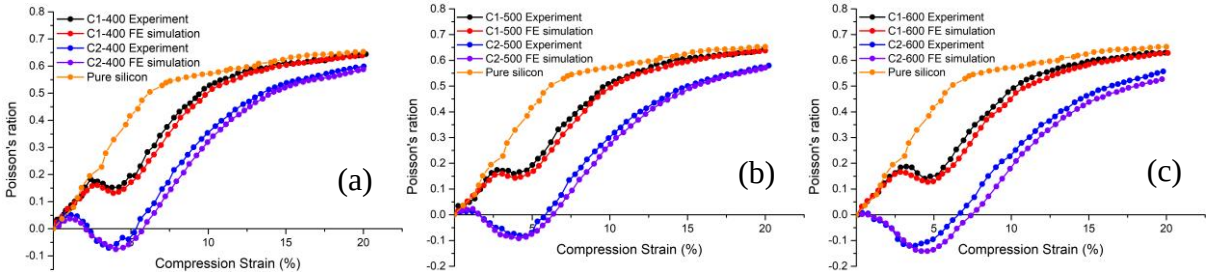

Fig. 8 PR-compression strain curves of the composites made from different fibre prepregs: (a) 400 inclusions, (b) 500 inclusions, (c) 600 inclusions.

4.4. Effect of prism length

Fig.9 shows both the experimental and FE simulated PR-compression strain curves of the composites (C2-400 to C2-600 and C3-400 to C3-600) made with the inclusions having the same re-entrant angle, the same rib thickness and made with the same carbon fibre prepreg but with different prism lengths (6mm and 8mm). It can be seen that the increase of prism length

of inclusion can result in the increase of PR, which makes C3 composites to lose their auxetic effect. Although the experimental results show that C3-600 composite has very small NPR at 4% compression strain due to higher inclusion numbers, the FE simulated results are positive. As shown in Eq. (1), with increasing the prism length of inclusions, the bending rigidity of the inclusion at the re-entrant point increases, which leads to reduced flexibility of the inclusion. Thus, higher compression force is required to deform the inclusions of C3 composites. When the compression force is high enough for the inward deformation of inclusions in C3 composites, the silicone matrix has expanded to a large extent, and the inward deformation of inclusions cannot provide sufficient lateral contraction for the composite to achieve NPR. On the other hand, although the increase of inclusion prism length can increase void space, the inconsistent inward deformation of inclusions also increases, which can result in a reduction of the lateral contraction of the composite.

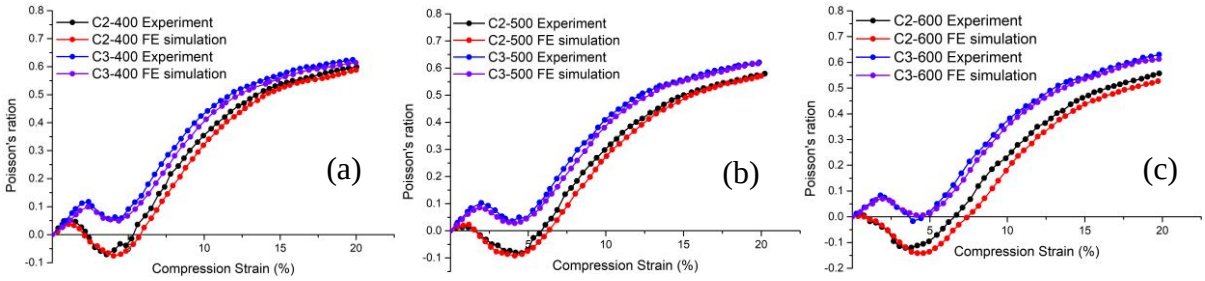

Fig. 9 PR-compression strain curves of composites with different prisms lengths of inclusions: (a) 400 inclusions, (b) 500 inclusions, (c) 600 inclusions.

4.5. Effect of re-entrant angle

Both the experimental and FE simulated PR-compression strain curves of the composites (C2-400 to C2-600 and C4-400 to C4-600 composites) made with the inclusions having the same rib thickness, the same prism length and made with the same carbon fibre prepregs but with different re-entrant angles (149° and 159°) are presented in Fig.10. It can be seen from the experimental results that the NPRs of two groups of composites almost have the same variation trend with compression strain. Their minimal and maximal PRs are close to each other. It is

difficult to find which re-entrant degree is providing better auxetic effect to the composites. Therefore, the influence of re-entrant angle on the auxetic effect of 3D auxetic composites is not evident from the experimental results. However, from the FE results, it can be observed that the C2 composites made with the inclusions of 149° re-entrant angle show lower PR values than C4 composites with the inclusions of 159° re-entrant angle. This is logic because inclusions with small re-entrant angle are easier to deform inward under compression, which increases the NPR. The difference between the experimental and FE simulated results may come from the inaccurate assembly of experimental inclusions. The cross-section of experimental inclusions may not be a perfect re-entrant equilateral triangle. The rib length and connecting angle may vary for each inclusion due to inaccurate cutting and bonding, which reduces the differences between two types of inclusions. Due to the limitation of manufacturing technique, the re-entrant angles could not be made with a larger gap to show clearer differences.

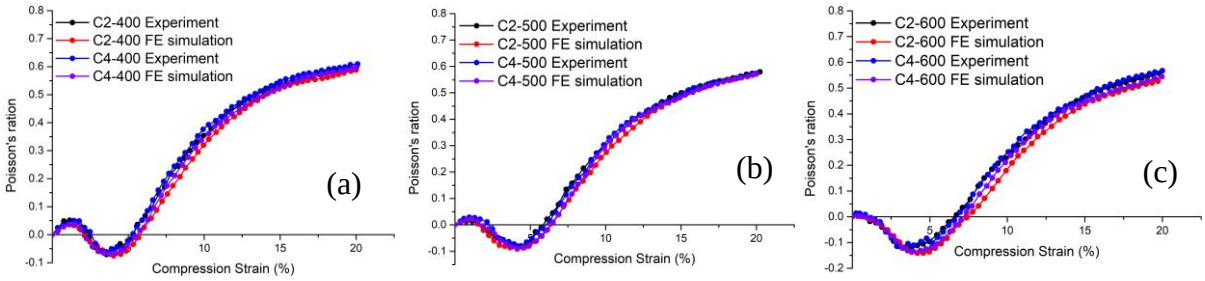

Fig. 10 PR-compression strain curves of composites with different re-entrant angles of inclusions: (a) 400 inclusions, (b) 500 inclusions, (c) 600 inclusions.

4.6. Compression properties

The compression stress-strain curves of all types of composites are shown in Fig. 11(a)-(d), in which the stress-strain curve of the pure silicone rubber is also included for comparison. It can be seen that the compression stress is almost linearly increased with the compression strain. The embedding of re-entrant inclusions can result in an increase of the compression properties of the composites, especially the compressive moduli of the composites increase with the increase of inclusion numbers. As shown in Fig. 11(e), the compressive modulus of the silicone

is 2.67 MPa. The embedding of 600 inclusions of Type I or II can increase this value to 3.5MPa, about an increase of 31%. However, due to low the volume fraction of inclusion shell, the enhancement of the compression properties of the composites is still limited. To further enhance the compression properties of the composites, it is necessary to continue to increase the volume fraction of inclusion shell. However, due to the limitation of the manufacturing process, the increase of the volume fraction of inclusion shell is limited. In addition, the increase of volume fraction of inclusion sell will need to increase inclusion number, making random distribution of inclusions in the matrix much more difficult. Meanwhile, the materials of inclusions can also influence the compression properties of the composites. As listed in Table 1, the 3-layers 1K carbon fibre reinforced laminate used for C1 composites has higher moduli than 1-layer 3K carbon fibre reinforced laminate. As a result, the C1 composites demonstrate around 9% higher compressive moduli than the counterparts of C2 composites. Furthermore, the increase of inclusion length can increase the volume fraction of inclusion shell, thus increase the compression moduli of the composites. The compressive moduli of C3 composites are 8% higher than C2 composites due to longer inclusion size.

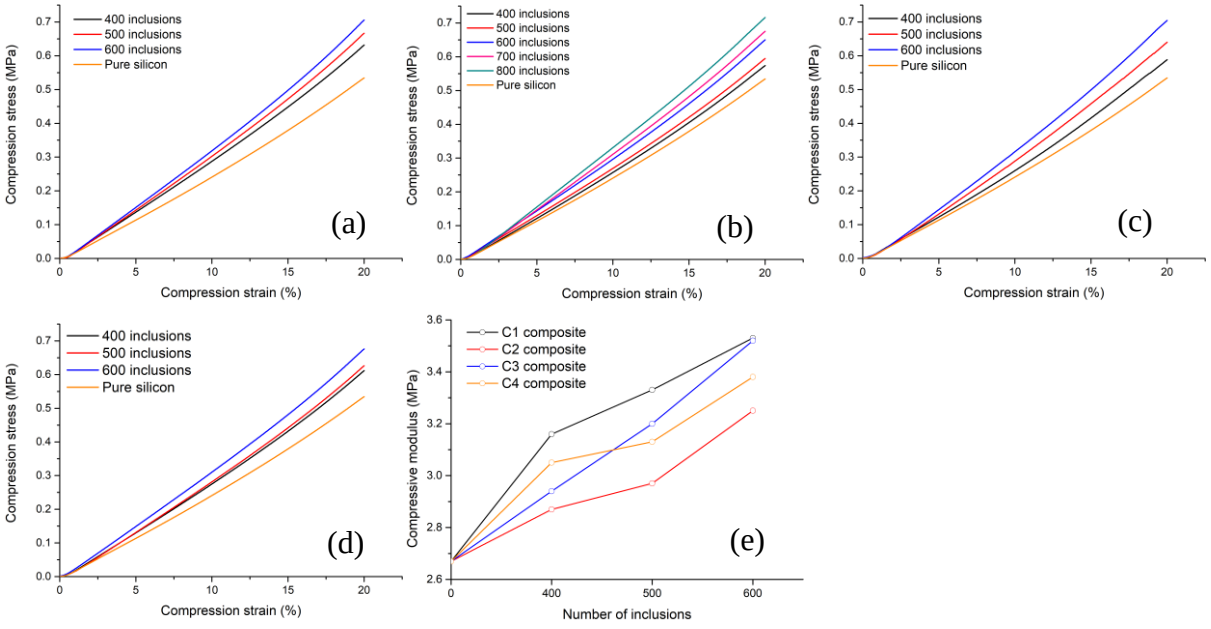

Fig. 11 Compression stress-strain curves: (a) C1 composites, (b) C2 composites, (c) C3 composites, (d) C4 composites, (e) compressive moduli of all composites.

5. Conclusions

Different types of re-entrant equilateral triangle inclusions were first made with different structural parameters and fibre prepregs and then used to make 3D composites with silicone rubber as matrix. Both the experiment and FE simulation were conducted to investigate the deformation behaviour of the composites manufactured under compression and the effects of structural parameters and carbon fibre prepregs. From the study, these conclusions can be obtained. 1) With suitable structural parameters, properties and numbers of inclusions, the 3D composites embedded with anisotropic re-entrant triangle inclusions can achieve nearly isotropic NPR during the initial stage of compression. 2) The NPR and the range of compression strain having NPR increase with the increase of inclusion number, but too many inclusions will cause overcrowding and extra expansion of the composite when compressed. To get the NPR of the composites, the inclusion number should exceed a minimum number when other parameters are kept unchanged. 3) The deformation behaviour of the composites is strongly affected by the structural parameters and material used of inclusions. 4) The compression properties can be enhanced with embedding of inclusions.

Acknowledgement

This work was supported by the Hong Kong PhD Fellowship Scheme from the Research Grants Council of Hong Kong Special Administrative Region Government. The authors would like to acknowledge help from the Industrial Centre of the Hong Kong Polytechnic University. The authors would like to thank the funding support from the Research Grants Council of Hong Kong Special Administrative Region Government for the NSFC/RGC Joint Research Scheme (Grant number: N_PolyU516/20).

Reference

1. Lakes R. Foam structures with a negative Poisson's ratio. Science. 1987; 235:1038-41.

2. Evans K, Nkansah M, Hutchinson I, Rogers S. Molecular network design. Nature. 1991; 353(6340):124-.

3. Lakes R, Elms K. Indentability of conventional and negative Poisson's ratio foams. Journal of Composite Materials. 1993; 27(12):1193-202.

4. Madke RR, Chowdhury R. Anti-impact behavior of auxetic sandwich structure with braided face sheets and 3D re-entrant cores. Composite Structures. 2020; 236:111838.

5. Scarpa F, Ciffo L, Yates J. Dynamic properties of high structural integrity auxetic open cell foam. Smart Materials and Structures. 2003; 13(1):49.

6. Novak N, Starčevič L, Vesenjak M, Ren Z. Blast response study of the sandwich composite panels with 3D chiral auxetic core. Composite Structures. 2019; 210:167-78.

7. Choi J, Lakes R. Non-linear properties of polymer cellular materials with a negative Poisson's ratio. Journal of Materials Science. 1992; 27(17):4678-84.

8. Evans K. The design of doubly curved sandwich panels with honeycomb cores. Composite Structures. 1991; 17(2):95-111.

9. Carneiro VH, Meireles J, Puga H. Auxetic materials—A review. Materials Science-Poland. 2013; 31(4):561-71.

10. Evans KE, Alderson A. Auxetic materials: functional materials and structures from lateral thinking! Advanced Materials. 2000; 12(9):617-28.

11. Saxena KK, Das R, Calius EP. Three decades of auxetics research− materials with negative Poisson's ratio: a review. Advanced Engineering Materials. 2016; 18(11):1847-70.

12. Milton GW. Composite materials with Poisson's ratios close to—1. Journal of the Mechanics and Physics of Solids. 1992; 40(5):1105-37.

13. Alderson K, Simkins V, Coenen V, Davies P, Alderson A, Evans K. How to make auxetic fibre reinforced composites. Physica Status Solidi (b). 2005; 242(3):509-18.

14. Herakovich CT. Composite laminates with negative through-the-thickness Poisson's ratios. Journal of Composite Materials. 1984; 18(5):447-55.

15. Alderson K, Coenen V. The low velocity impact response of auxetic carbon fibre laminates. Physica Status Solidi (b). 2008; 245(3):489-96.

16. Zhang R, Yeh H-L, Yeh H-Y. A preliminary study of negative Poisson's ratio of laminated fiber reinforced composites. Journal of Reinforced Plastics and Composites. 1998; 17(18):1651-64.

17. Miller W, Hook P, Smith CW, Wang X, Evans KE. The manufacture and characterisation of a novel, low modulus, negative Poisson's ratio composite. Composites Science and Technology. 2009; 69(5):651-5.

18. Miller W, Ren Z, Smith C, Evans K. A negative Poisson's ratio carbon fibre composite using a negative Poisson's ratio yarn reinforcement. Composites Science and Technology. 2012; 72(7):761-6.

19. Liaqat M, Samad HA, Hamdani STA, Nawab Y. The development of novel auxetic woven structure for impact applications. The Journal of the Textile Institute. 2017; 108(7):1264-70.

20. Boakye A, Raji RK, Ma P, Cong H. Compressive property of an auxetic-knitted composite tube under quasi-static loading. Autex Research Journal. 2020; 20(2):101-9.

21. Shufrin I, Pasternak E, Dyskin AV. Hybrid materials with negative Poisson's ratio inclusions. International Journal of Engineering Science. 2015; 89:100-20.

22. Assidi M, Ganghoffer JF. Composites with auxetic inclusions showing both an auxetic behavior and enhancement of their mechanical properties. Composite Structures. 2012; 94(8):2373-82.

23. Poźniak AA, Wojciechowski KW, Grima JN, Mizzi L. Planar auxeticity from elliptic inclusions. Composites Part B: Engineering. 2016; 94:379-88.

24. Jiang L, Gu B, Hu H. Auxetic composite made with multilayer orthogonal structural reinforcement. Composite Structures. 2016; 135:23-9.

25. Li T, Liu F, Wang L. Enhancing indentation and impact resistance in auxetic composite materials. Composites Part B: Engineering. 2020; 198:108229.

26. Quan C, Han B, Hou Z, Zhang Q, Tian X, Lu TJ. 3D printed continuous fiber reinforced composite auxetic honeycomb structures. Composites Part B: Engineering. 2020; 187:107858.

27. Novak N, Vesenjak M, Kennedy G, Thadhani N, Ren Z. Response of Chiral Auxetic Composite Sandwich Panel to Fragment Simulating Projectile Impact. Physica Status Solidi (b). 2020; 257(10):1900099.

28. Wang X-T, Wang B, Wen Z-H, Ma L. Fabrication and mechanical properties of CFRP composite three-dimensional double-arrow-head auxetic structures. Composites Science and Technology. 2018; 164:92-102.

29. Gao Y, Zhou Z, Hu H, Xiong J. New concept of carbon fiber reinforced composite 3D auxetic lattice structures based on stretching-dominated cells. Mechanics of Materials. 2021; 152:103661.

30. Gao Y, Wu Q, Wei X, Zhou Z, Xiong J. Composite tree-like re-entrant structure with high stiffness and controllable elastic anisotropy. International Journal of Solids and Structures. 2020; 206:170-82.

31. Assidi M, Ganghoffer J-F. Composites with auxetic inclusions showing both an auxetic behavior and enhancement of their mechanical properties. Composite Structures. 2012; 94(8):2373-82.

32. Kochmann DM, Venturini GN. Homogenized mechanical properties of auxetic composite materials in finite-strain elasticity. Smart Materials and Structures. 2013; 22(8):084004.

33. Hou X, Hu H, Silberschmidt V. A novel concept to develop composite structures with isotropic negative Poisson's ratio: Effects of random inclusions. Composites Science and Technology. 2012; 72(15):1848-54.

34. Hu H, Silberschmidt V. A composite material with Poisson's ratio tunable from positive to negative values: An experimental and numerical study. Journal of Materials Science. 2013; 48(24):8493-500.

35. Hou X, Hu H. A novel 3D composite structure with tunable Poisson's ratio and stiffness. Physica Status Solidi (b). 2015; 252(7):1565-74.

Figure Captions

Fig. 12 (a) Re-entrant equilateral triangle inclusion, (b)deformation of the re-entrant triangle.

Fig. 2 (a) Schematic diagram showing the manufacturing process of 3D auxetic composite, (b) schematic diagram of the wave-surface mould, (c) cross-section of the mould.

Fig. 13 (a) Experimental setup of the compression test, (b) composite under compression.

Fig. 14 (a) Model of the auxetic composite embedded with inclusions, (b) FE model for compression tests, (c) FE model without matrix.

Fig. 15 PR-compression strain curves of C2-500 composite along x, y and z directions.

Fig. 16 Deformations of C2-500: (a) and (b) test and FE simulation at 4% compression strain, (c) and (d) test and FE simulation at 15% compression strain.

Fig. 7 (a) and (b) FE simulated and experimentally measured PR-compression strain curves with different inclusion numbers, (c) variation of the largest NPR with inclusion numbersFig. 17 PR-compression strain curves of the composites made from different fibre prepregs: (a) 400 inclusions, (b) 500 inclusions, (c) 600 inclusions.

Fig. 18 PR-compression strain curves of composites with different prisms lengths of inclusions: (a) 400 inclusions, (b) 500 inclusions, (c) 600 inclusions.

Fig. 19 PR-compression strain curves of composites with different re-entrant angles of inclusions: (a) 400 inclusions, (b) 500 inclusions, (c) 600 inclusions.

Fig. 20 Compression stress-strain curves: (a) C1 composites, (b) C2 composites, (c) C3 composites, (d) C4 composites, (e) compressive moduli of all composites.

Declaration of interests

☒ The authors declare that they have no known competing financial interests or personal relationships that could have appeared to influence the work reported in this paper.

☐The authors declare the following financial interests/personal relationships which may be considered as potential competing interests:

Author statement

Minglonghai Zhang: Conceptualization, Methodology, Validation, Formal analysis, Investigation, Software, Writing-Original Draft; **Hong Hu**: Conceptualization; Methodology, Writing-Review& Editing; Supervision; Funding acquisition; **Hasan Kamrul**: Methodology, Investigation; **Shuaiquan Zhao**: Investigation; **Yuping Chang**: Investigation; **Mabel Ho**: Investigation; **Nazmul Karim**: Writing - Review & Editing.